Received: 13 November 2019 | Revised: 19 January 2020 | Accepted: 22 January 2020

DOI: 10.1002/rra.3600

RESEARCH ARTICLE

WILEY

Hybrid modelling of low velocity zones in an asymmetrical channel with sidewall longitudinal rib to assist fish passage

Pedro X. Sanchez | Xinqian Leng | Johann Von Brandis-Martini | Hubert Chanson

School of Civil Engineering, The University of Queensland, Brisbane, Australia

Correspondence
Xinqian Leng, School of Civil Engineering, The University of Queensland, Brisbane QLD 4072, Australia.
Email: xinqian.leng@uqconnect.edu.au

Funding information
Australian Research Council, Grant/Award Number: LP140100225

Abstract

Channels with longitudinal beams have been studied for decades in chemical engineering, environmental and sanitary engineering, aeronautics, astronautics, biology and geology. In the current study, a combination of physical and numerical Computational Fluid Dynamics (CFD) modelling was undertaken to test whether an asymmetrical channel equipped with a sidewall longitudinal rib could provide flow conditions conducive to upstream fish passage. The study focused on small-bodied fish and juveniles of larger fish, typically less than 100 mm in total length. A detailed hydrodynamic study was conducted in an asymmetrical rectangular channel equipped with a sidewall square rib in a culvert barrel channel. Both free-surface velocity and boundary shear stress measurements showed strong secondary currents of Prandtl's second kind. The channel asymmetry contributed to intense secondary motion, associated with turbulent dissipation. The channel design provided a small well-defined highly turbulent low-velocity zone beneath the rib. In the context of hydraulic structure designs, uttermost care must be considered because of manufacturing, installation and operational practices. In many instances, alternative engineering designs with small baffles and asymmetrical appurtenance should be preferred to assist with fish passage in hydraulic structures.

KEYWORDS

culvert, fish passage, hydraulic modelling, hydrodynamics, longitudinal rib, remediation

1 | INTRODUCTION

In alluvial channels, long-lasting three-dimensional large-scale turbulent vortices may yield the development of longitudinal troughs and ridges on the mobile bed with preferential transport of bed particles along troughs (Nezu & Nakagawa, 1984; Shvidchenko & Pender, 2001). Longitudinal ridges and runnels were also reported in intertidal zones (Carling, Williams, Croudace, & Amos, 2009). Related observations include massive scour features, with longitudinal ridges and grooves, and streamlined bar forms, in debris flows on Planet Mars (Tanaka, 1999). Small-scale streamwise ribs, also called V-groove riblets, can produce consistent net drag reduction, when the appropriate groove spacing yields a reduction in viscous drag by displacing longitudinal vortices away from the wetted surface, thus reducing their intensity (Bushnell & McGinley, 1989; Choi, Moin, & Kim, 1993). The scales of fast-swimming sharks have fine longitudinal ridges, comparable to grooves and riblets, which reduce the flow resistance of a surface, enabling drag reduction and faster swimming (Nitschke, 1983). A related application is the flow past seal fur, achieving drag reductions of up to 12%, due to the streamwise fur pattern (Itoh et al., 2006).

Recent biological tests suggested that a streamwise rib might facilitate the upstream passage of small-body-mass fish species (Watson, Goodrich, Cramp, Gordos, & Franklin, 2018). The longitudinal rib would typically be placed along each river bank, that is, on one sidewall of the outer cells of multi-cell box culverts; or on both sidewalls of a single-cell box culvert. The purpose of the present hydrodynamic investigation is to characterise the role of longitudinal rib on the flow field in a rectangular channel, typical of a standard box culvert barrel, to gain some fundamental understanding of the implications in terms of turbulent mixing and to develop a physically based understanding of the potential impact in terms upstream passage of small-bodied fish and juveniles of large fish species, although the impact on fish behaviour and passage was not tested. Engineering design considerations are later discussed.

2 | MODELLING AND HYDRODYNAMIC CONDITIONS

2.1 | Physical modelling

New experiments under controlled flow conditions were conducted in a 15-m long 0.5-m wide horizontal flume at the Advanced Engineering Building (AEB) Hydraulics Laboratory of the University of Queensland (Figure 1). In Australia, the large majority of box culverts use pre-cast concrete boxes with internal widths between 0.5 and 2.5 m. Thus, the present channel test section had similar dimensions to those of a real standard box culvert barrel cell beneath a two-lane road, allowing some quasi 1:1 scale prototype-model testing.

The test section was made of a smooth Polymerizing Vinyl Chloride (PVC) bed and glass sidewalls. Water was supplied by a constant head tank into the flume intake, in which the combination of baffles, vanes and three-dimensional convergent allowed a smooth inflow into the 15-m long flume, which ended with a free overfall at the downstream end.

A 12-m long sidewall rib was installed along the right sidewall for 1 m < x < 13 m, with x is the streamwise distance from the upstream end of the test section (Figure 1a,b). The rib dimensions and position are shown in Figure 2 and were based upon Watson et al. (2018), albeit with stringent tolerance in terms of dimensions and installation (Sanchez, Leng, & Chanson, 2018).

The discharge was recorded with a Venturi meter on the water delivery line, with an accuracy of less than 2%. Water depths were measured with rail-mounted pointer gauges within ±0.5 mm. Water velocities were recorded with a combination of three systems: a Prandtl-Pitot tube, a roving Preston tube (RPT) and an acoustic Doppler velocimeter (ADV). The Prandtl-Pitot tube was a Dwyer® 166 Series tube (Ø 3.18 mm), with an AMCA/ASHRAE design. The RPT was a Type C1.6(r) (Macintosh & Isaacs, 1992), especially used to measure the velocity beneath the square rib (Figure 1c). With the Prandtl-Pitot tube, the percentage of error was expected to be less than 2% on the time-averaged velocity measurement. The accuracy of the RPT was basically similar. The ADV was a Nortek™ Vectrino+ with a three-dimensional side-looking head. The ADV signals were post-processed by removing erroneous data with an average correlation of less than 60% and an average Signal to Noise Ratio (SNR) less than 5 dB, as well as by "despiking" using a phase-space thresholding technique (Goring & Nikora, 2002). Note that the ADV signal was adversely affected by the proximity of solid boundaries, especially the corners and edges of the longitudinal rib (Figure 1d). Although the accuracy of the ADV was supposedly 1% of the velocity range, that is, 0.01 m/s herein, great care should be applied to the interpretation of these data (Sanchez et al., 2018).

2.2 | Numerical CFD modelling

Numerical CFD modelling was performed using ANSYS™ Fluent version 18.0. The numerical CFD model was constructed following closely the experimental configuration, using a 12-m long 0.5-m wide numerical domain with caved-in wall element along the right sidewall resembling the longitudinal rib (Figure 3). The corner of the numerical rib was square and sharp as shown in Figure 3 (right), based upon the physical model. The upstream boundary was configured as two velocity inlets, being air and water, respectively, separated by a free-surface elevation at z = 0.165 m, according to the experimental measurements at the upstream end of the test section. The inflow velocity of air was zero, whereas for water V_{in} = 0.674 m. The downstream boundary was configured as a pressure outlet with a prescribed free-surface elevation at z = 0.135 m according to experimental observations near the downstream end. The total height of the numerical domain was 0.5 m. The rest of the boundaries, including top, sidewalls and sides of the rib, applied wall boundary conditions with a consistent roughness height comparable to smooth PVC channel (k_s ~ 0). The numerical model aimed to simulate the flow condition tested by the experimental model: Q = 0.0556 m^3/s.

Even with such a large streamwise element intruding the flow, the flow remained a gradually varied steady nontransient flow due to the uniformity of the beam's shape extending throughout the test section. Strong side-current and streamline distortion were expected near the edge of the rib; however, minimum separation was anticipated, except maybe near the sharp corners of the rib, which was not the focus of this study. Hence, a Reynolds-averaged Navier–Stokes (RANS) simulation was selected for modelling turbulence in the numerical model (Pope, 2000; Rodi, Constantinescu, & Stoesser, 2013). Two RANS models were tested, which were a standard k-ε model and a Reynolds stress model (RSM). The latter is considered more powerful in resolving complicated flow field, including anisotropic turbulence, streamline curvature, swirl, rotation and rapid changes in strain rate, hence more suitable for the purpose of current study (Pope, 2000, Rodi et al., 2013). A two-phase volume of fluid method was used for both turbulence models to resolve the air–water interface. A segregated pressure–velocity coupling was used (SIMPLE). The momentum spatial discretisation was solved by a second-order upwind scheme and the time discretisation was solved using a first-order implicit scheme.

For both $k - \varepsilon$ and RSM, a structured hexagon mesh was employed. Example of cross-sectional mesh configuration is shown in Figure 4. Minimum edge sizing was applied for the water phase being the focus of this study, with Δy_{min} and Δz_{min} = 0.0025 m. In the air phase, a gradually varied rectangular mesh was used, with Δy_{min} and Δz_{min} = 0.0025 m. The longitudinal mesh was mostly uniformly partitioned with Δx = 0.6 m. Overall the mesh grid consisted of 119,922 nodes and 107,505 elements. A refined mesh was tested further using RSM only to examine the sensitivity of the method to mesh grid density. A cross-section of the refined mesh is shown in Figure 4b, with Δy_{min} = 0.001, Δz_{min} = 0.001 and Δx = 0.6 m. The total mesh grid density was 375,717 nodes and 342,550 elements.

Transient simulation was performed for all numerical models. Convergence was achieved by reducing residuals of all parameters to 10^{-3} or less. The physical time of each model was 120 s to ensure the flow

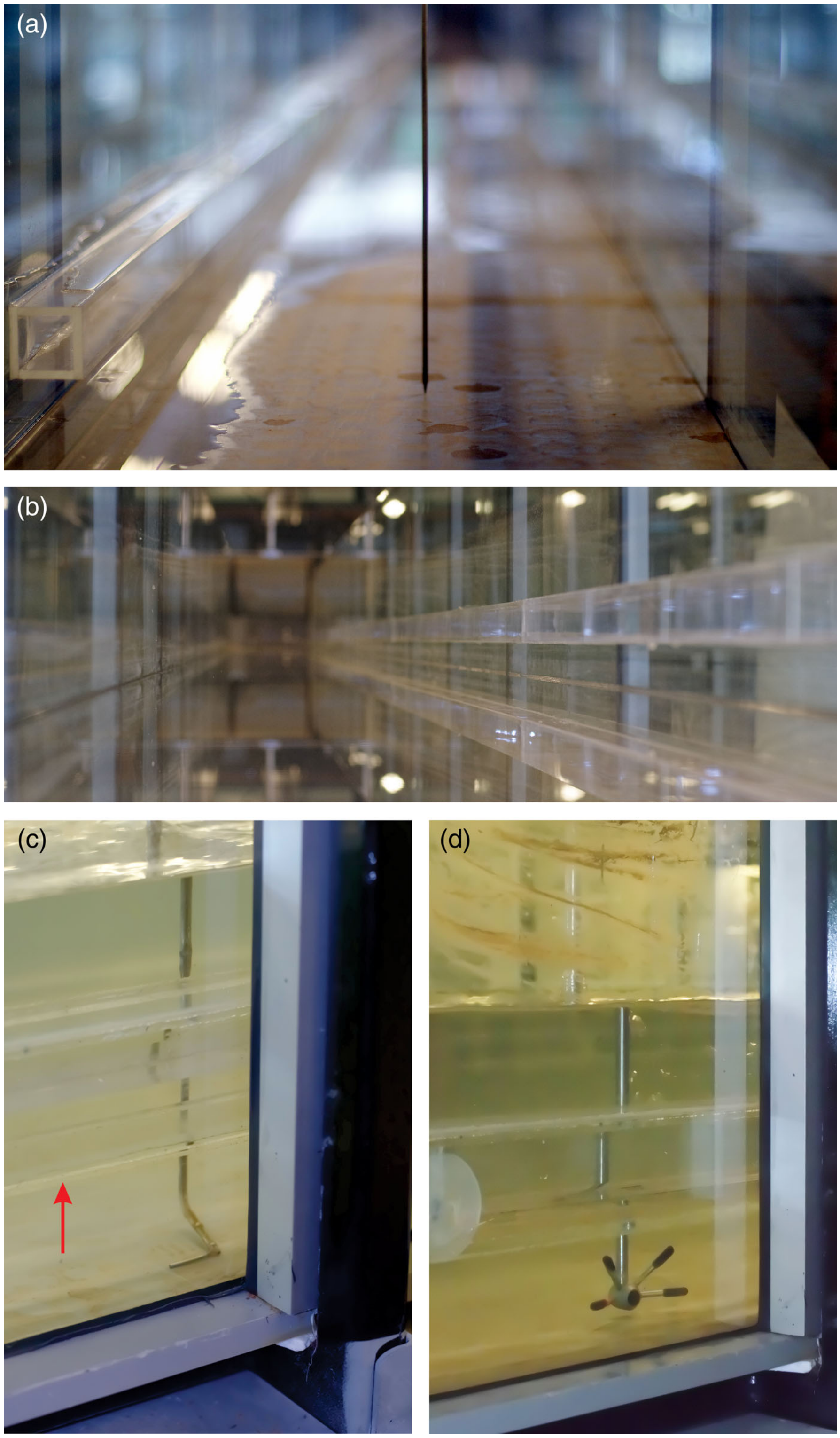

FIGURE 1 Photographs of the physical facility with 50 mm^2 × 50 mm^2 longitudinal rib along a right sidewall. (a) Looking upstream at the downstream end of the hollow rib (white arrow) with a pointer gauge on the dry channel bed. (b) Looking downstream at the dry flume with the longitudinal rib along the right sidewall. (c) Roving Preston tube (RPT) Type C1.6 (r) underneath the longitudinal rib (red arrow). (d) Acoustic Doppler velocimeter (ADV) with the head facing the right sidewall, beneath the longitudinal rib. Flow direction from left to right—Q = 0.0556 m^3/s [Colour figure can be viewed at wileyonlinelibrary.com]

became steady. The computation time for each model was 24–48 hr on an eight-processor High Performance Computer (HPC) workstation.

2.3 | Hydrodynamic flow conditions

Physical experiments were performed in the horizontal channel, equipped with a sidewall longitudinal square rib for a range of discharges. Visual observations and free-surface measurements were conducted every meter along the longitudinal length of the flume. Detailed velocity measurements were undertaken for one flow rate: Q = 0.0556 m^3/s at three longitudinal locations (x = 1.9, 8 and 11.9 m), as well as several transversal locations y, where y is the transversal distance from the right sidewall, positive towards the left sidewall. Each vertical velocity profile consisted of a minimum of 25 points, with typically over

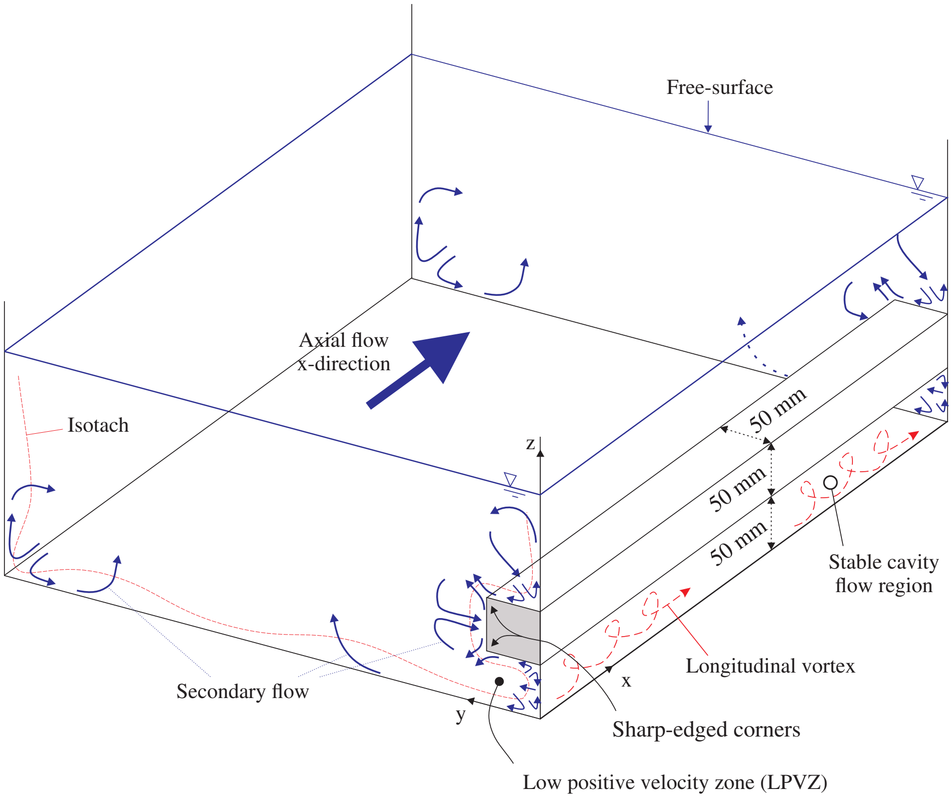

FIGURE 2 Undistorted sketch of streamflow, recirculation cavity and secondary flows in an asymmetrical box culvert barrel with sidewall longitudinal rib with sharp-edged corners [Colour figure can be viewed at wileyonlinelibrary.com]

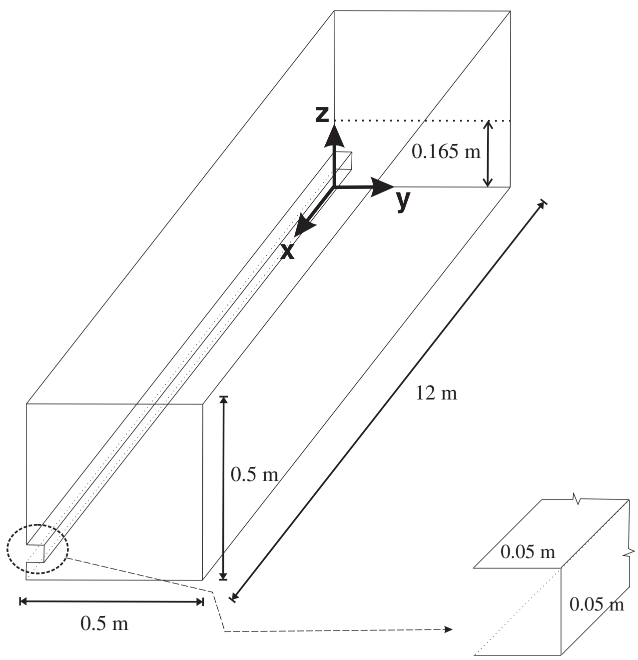

FIGURE 3 Distorted sketch of the numerical domain (left) with a zoom on the rib section (right)

350 velocity sampling points per cross-section. Further velocity measurements were also conducted for Q = 0.026 and 0.100 m^3/s at x = 8 m to characterise the low-velocity zones (LVZs).

3 | FLOW PATTERNS AND VELOCITY FIELD

3.1 | Basic flow regimes

Basic experiments were conducted for a range of flow rates 0.008 $m^3/s < Q <$ 0.100 m^3/s. Such flows corresponded to a subcritical flow motion, typical of less-than-design discharges in a box culvert. For all discharges, the flow was quasi-uniform at the beginning of the channel. The effect of boundary friction developed with increasing longitudinal distance. Detailed velocity measurements, performed at three different longitudinal locations, demonstrated that the velocity field became fully developed between 2 m < x < 8 m. Photographic observations, including dye injection experiments, showed limited mixing between the main flow and the cavity region underneath the longitudinal rib. The cavity flow was further the locus of long-lasting helicoidal vortices with longitudinal axis, as sketched in Figure 2.

Ignoring the trivial case when the water surface did not touch the rib (Q < 0.012 m^3/s), three flow situations were observed. For 0.050 m < d < 0.100 m, with d the water depth, the sidewall longitudinal rib interacted with the free surface, which was then narrower. Flow visualisations by dye injection showed that the rib pushed the high-velocity flow region towards the smooth (left) sidewall. For 0.100 m < d < 0.150 m, the water level above the upper face of the rib was shallow, and the flow there was decelerated as a combination of boundary friction and corner flows. The high-velocity region tended to be closer to the left wall. At large discharges, that is,

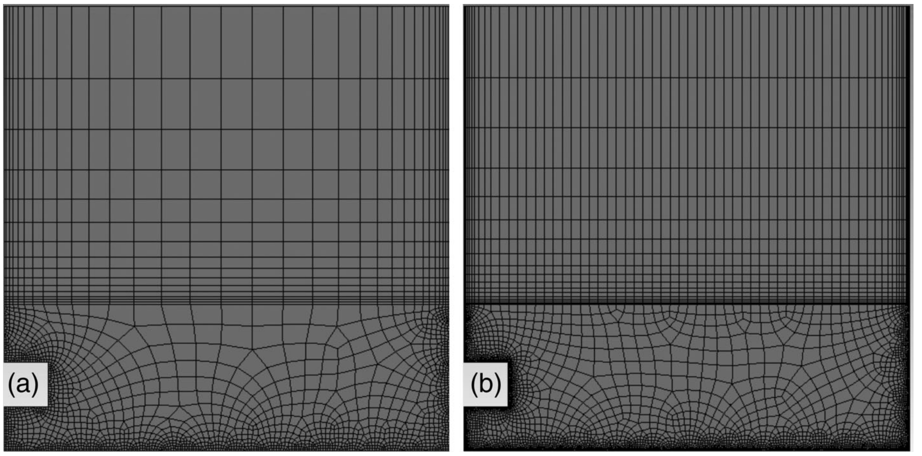

FIGURE 4 An example of meshing on the cross-section of numerical model ($k-\varepsilon$ and RSM); a refined mesh is shown on the right-hand side (RSM only). (a) Cross-sectional meshing for $k-\varepsilon$ and RSM. (b) Refined mesh for RSM. RSM, Reynolds stress model

d < 0.150 m, the bulk of the flow was little affected by the longitudinal rib, while the fluid flow in the square cavity beneath the right sidewall rib was always slower than the main flow.

3.2 | Velocity measurements

Detailed velocity measurements were conducted in the sidewall ribbed channel section, using a combination of velocimeters. The longitudinal velocity V_x results are presented in this section. Typical results are shown in Figure 5.

The longitudinal rib impacted onto the velocity field. For large discharges and z > 0.1 m, large velocities were observed about the centreline of the flume as illustrated in Figure 5, with z the vertical distance from the bed of the flume. For z < 0.1 m, the high-velocity region was shifted towards the left smooth wall, as a result of the spanwise asymmetry. Low-velocity regions were observed in the cavity beneath the rib. Overall, some complex velocity pattern was observed near the edges of the rib, evidences of strong secondary currents. For Q = 0.0556 m^3/s, measurements at three longitudinal locations showed a quasi-uniform velocity field at the upstream end of the flume, that is, at 0.9 m from the start of the rib, where the boundary layer regions were not fully developed (Figure 5a). At the downstream end of the ribbed channel (x = 11.9 m), the velocity distributions were fully developed, with a shape similar to that observed at x = 8 m (Figure 5c). The longitudinal velocities in the cavity beneath the rib increased by about 20–25% from the upstream end to the downstream end of the rib, in line with the increase in cross-sectional averaged velocity V_{mean} from x = 1.9–11.9 m.

The LVZ underneath the sidewall rib was well-defined albeit small. For Q = 0.0556 m^3/s, the longitudinal velocities in the cavity beneath the rib were about 0.5–0.7 m/s, or $0.75 \times V_{mean}$, with V_{mean} is the average cross-sectional velocity. Longitudinal velocities below $0.75 \times V_{mean}$ covered around 18% of the cross-sectional area of the flume. Data from experiments conducted under similar flow rates by Cabonce, Fernando, Wang, and Chanson (2017, 2019) and Wang, Uys, and Chanson (2018) showed longitudinal velocities below $0.75 \times V_{mean}$ covering areas between 21% and 32%. Compared to these configurations, the sidewall rib geometry appeared to produce lesser LVZ areas.

Velocity fluctuations, recorded using an ADV showed large meaningless longitudinal and vertical velocity fluctuation outputs, suggesting possible errors. Errors might have been caused by a combination of insufficient seeding of the water reticulation system, and the proximity of solid boundaries, especially the inner and outer corners of the rib. The transverse velocity fluctuations appeared to be less affected. Very large transverse velocity fluctuations were observed near the edges of the rib. Large turbulence levels were also seen in the low-velocity cavity region beneath the longitudinal rib. At low flow rates, the velocity fluctuations next to the rib edges were relatively small, but increased substantially with increasing flow rates. Overall the findings were consistent with strong secondary currents about the same locations (Figure 2).

3.3 | Numerical CFD modelling and validation

Numerical modelling was conducted following the experimental flow condition of the intermediate discharge (Q = 0.0556 m^3/s) using two RANS-based turbulence models—a standard $k-\varepsilon$ model and a RSM. Despite the intrinsic limitations of the standard $k-\varepsilon$ mode (Pope, 2000; Rodi, 1995), a direct comparison between $k-\varepsilon$ and RSM with detailed experimental validation may provide valuable insights to the specific limits of both turbulence models. Cross-sectional views of the longitudinal velocity contours taken at x = 8 m simulated by both models are shown in Figure 6a,b.

The CFD models showed a velocity range from 0 to 1 m/s, comparable to experimental results (Figure 5b). However, the area where V_x < 0.9 m/s was systematically underestimated by both CFD models at x = 8 m, compared to experimental data. Previous numerical studies of culvert flows simulated using RANS models in Fluent showed similar overestimations (Leng & Chanson, 2018, 2020; Zhang & Chanson, 2018b) in velocity increase outside of the boundary layer regions, sometimes up to 10% larger than the experimental reference. The CFD models also showed some large velocity dip near the free surface. A velocity dip is the decrease in longitudinal velocity near the

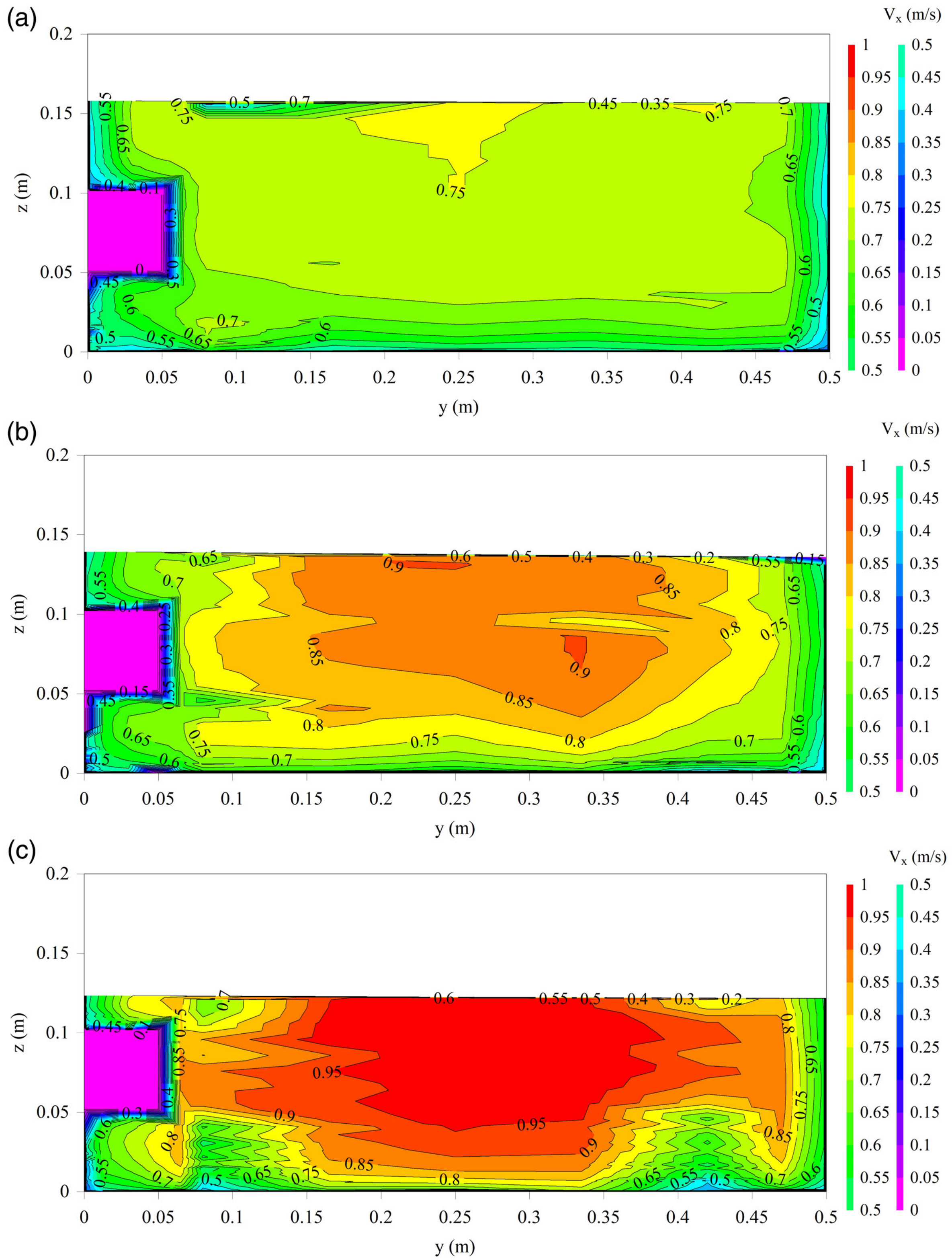

FIGURE 5 Contour plots for longitudinal velocity V_x (m/s) in the sidewall ribbed channel at x = 1.9 m (a), x = 8 m (b) and x = 11.9 m (c) for Q = 0.0556 m^3/s, looking upstream [Colour figure can be viewed at wileyonlinelibrary.com]

free surface due to presence of side currents. Herein, some degree of velocity dipping was observed in the experimental data (Figure 5), but not to the same extent as seen in Figure 6. In terms of wall boundary layers, both numerical models showed very good agreement with experimental observations for the left wall boundary and near-bed region. In the vicinity of the rib, RSM seemed to give better simulation

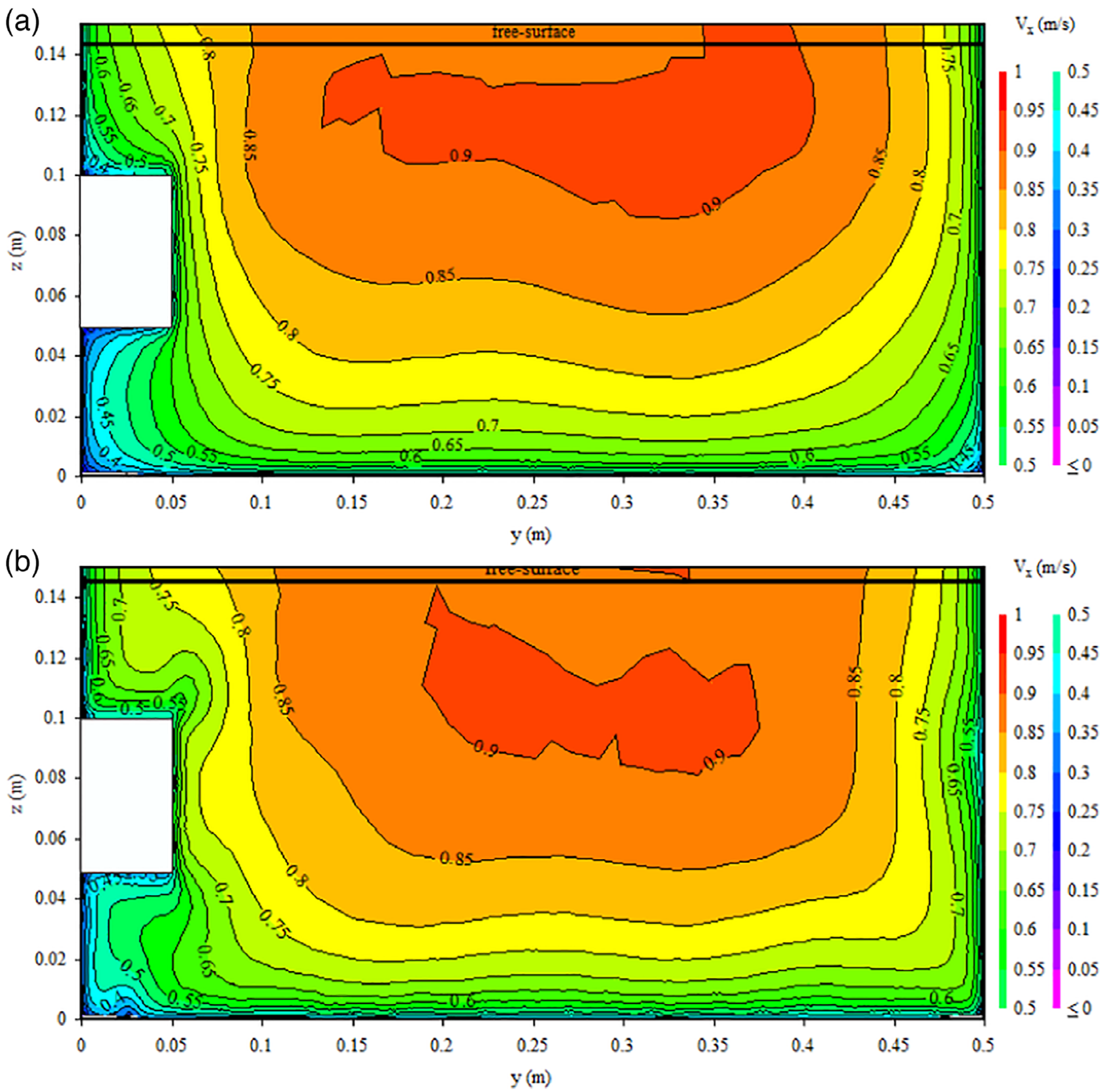

FIGURE 6 Contour plots for longitudinal velocity V_x (m/s) in the sidewall ribbed channel at x = 8 m simulated numerically using (a) a standard $k - \varepsilon$ and (b) Reynolds stress model for Q = 0.0556 m^3/s, looking upstream; black line indicating free-surface location [Colour figure can be viewed at wileyonlinelibrary.com]

near the lower edge, lower corners of the rib and the region in-between the rib, right side wall and channel bed (Figure 6b). However, the $k - \varepsilon$ model showed better approximation of the flow field near the upper edge, especially at the tip of the upper rib corner (Figure 6a), where the RSM data showed some marked rounding of the streamline at the tip of the corner that were not seen in the experimental data. Both models highlighted the asymmetrical nature of the flow field under the effect of the rib and a marked LVZ underneath the rib.

Further CFD modelling using a RSM on a refined mesh (Figure 4b) was performed to examine the effect of mesh on the numerical results. Detailed validation against experimental data at various longitudinal locations are presented in Figure 7. Overall, at the same longitudinal location (x = 8 m), the results showed little sensitivity to the mesh refinement, though more details were simulated near the wall boundaries. The problem with the RSM data near the upper rib edge was not solved by mesh refining. Experimental data at a higher flow rate Q = 0.1 m^3/s showed a similar flow feature near the upper edge, namely, a large streamline curvature around the tip of the upper edge, though not as rounded in shape as in the numerical data (Sanchez et al., 2018). The reason for this difference could be the different "sharpness" of the edge and corner of the rib. In the experiments, the rib corner was not a sharp object whereas for numerical model, the complete right-angled corner may be treated as a sharp edge, resulting in some degree of flow separation at the sharp front.

Near the upstream end of the culvert barrel channel (x = 2 m), the numerical results showed close quantitative agreement with experimental data. Towards the downstream end (x = 11 m), the comparison between numerical results to experiments was less satisfactory, possibly because of experimental issues (Figure 5c). Altogether, the flow

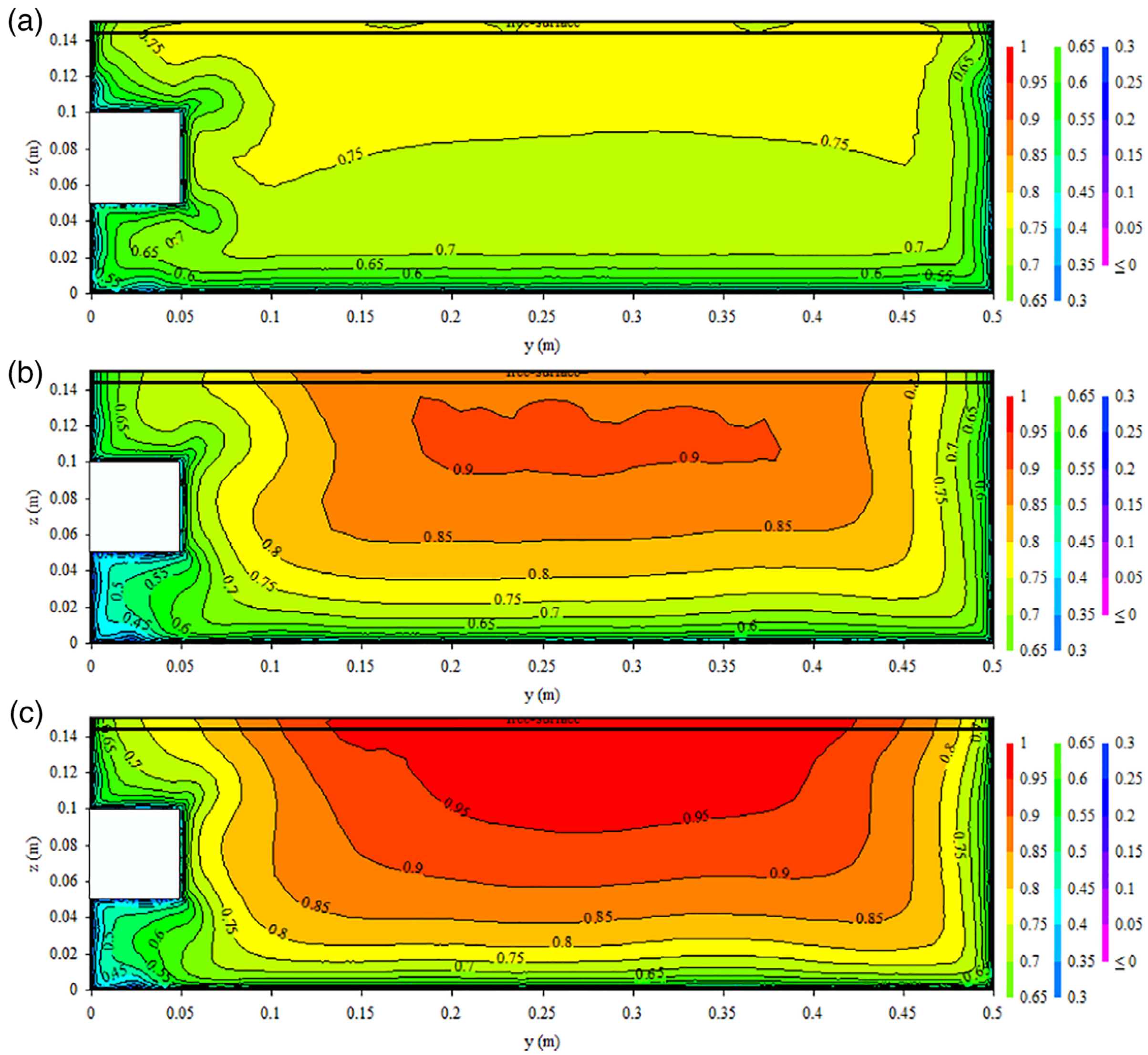

FIGURE 7 Contour plots for longitudinal velocity V_x (m/s) in the sidewall ribbed channel at x = 1.9 m (a), x = 8 m (b) and x = 11.9 m (c) simulated by Reynolds stress model with a refined mesh for Q = 0.0556 m^3/s, looking upstream; black line indicating free-surface location [Colour figure can be viewed at wileyonlinelibrary.com]

fields showed comparable velocity range, a well-marked LVZ underneath the rib, and an asymmetrical shape for both numerical and experimental results.

4 | BOUNDARY SHEAR STRESS

Boundary shear stress measurements were performed along the wetted perimeter in the ribbed channel using Preston tubes (Sanchez et al., 2018). Figure 8 presents dimensionless distributions of surface friction boundary shear stress along the wetted perimeter at three longitudinal locations, where f_{skin} is dimensionless skin friction shear stress and f is the dimensionless total boundary shear stress. The relationship between skin boundary shear stress and friction factor is

$$(\tau_o)_{skin} = \frac{f_{skin}}{8} \times \rho \times V_{mean}^2, \qquad (1)$$

with V_{mean} the bulk velocity. In Figure 8, $Y''$is the wetted perimeter coordinate, with Y'' = 0 at the bottom right corner of the flume (Figure 2), while the vertical lines represent the physical corners.

The data indicated a non-uniform distribution of surface shear stress (Figure 8). The boundary shear stress was asymmetrically distributed across the channel, with large shear stresses along the sidewall longitudinal rib. Such large shear stresses implied strong interactions between the main flow, secondary currents and cavity recirculation, as sketched in Figure 2. Figure 8 shows that the boundary shear stress distribution was more uniform at the upstream end of the ribbed channel (x = 1.9 m), where the boundary layer was partially developed. The boundary shear stress became less uniform as the flow developed.

Figure 9 shows the boundary shear data simulated by RSM on a refined mesh. Overall, the CFD data showed larger skin shear compared to the experimental data, except around the cavity underneath

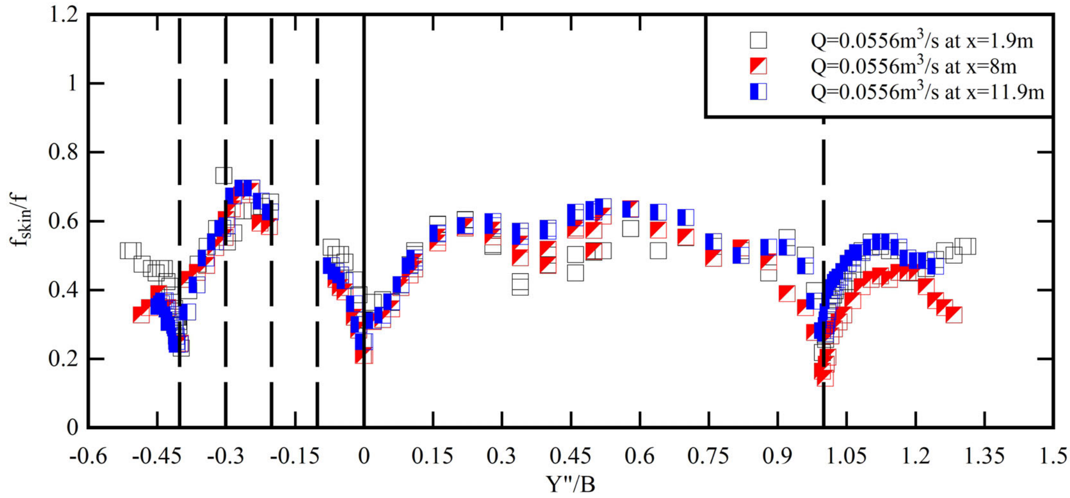

FIGURE 8 Distributions of dimensionless boundary shear stress f_{skin}/f along the wetted perimeter of the ribbed channel—flow conditions: Q = 0.0556 m^3/s, x = 1.9 m, 8 m, 11.9 m [Colour figure can be viewed at wileyonlinelibrary.com]

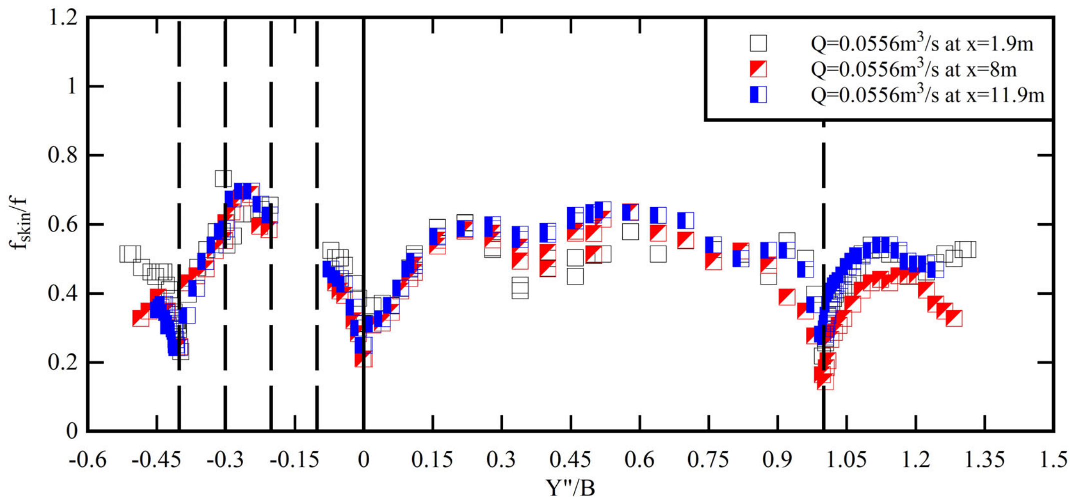

FIGURE 9 Distributions of dimensionless boundary shear stress f_{skin}/f along the wetted perimeter of the ribbed channel simulated using Reynolds stress model on a refined mesh—Flow conditions: Q = 0.0556 m^3/s, x = 8.2 m [Colour figure can be viewed at wileyonlinelibrary.com]

the rib. Qualitatively, the CFD results also highlighted higher shear along the vertical edge of the rib.

5 | DISCUSSION

5.1 | Low-velocity zones

The detailed velocity data were used to quantify the relative size of LVZs, associated with each flow rate. Figure 10 presents the results. Tabular data are reported in Table 1. Figure 10 shows the fraction of wetted cross-sectional area where the ratio of longitudinal velocity to mean velocity was V_x/V_{mean} < 0.3, 0.5, 0.75 and 1. Overall, the percentage of flow area where V_x/V_{mean} was less than 0.3 was less than 3%. The relative flow area where V_x/V_{mean} < 0.75 ranged from 16 to 25%. The results suggested drastic changes in LVZ sizes depending upon the definition of LVZ and the velocity target. The results were overall little affected by the discharge, within the experimental conditions. The numerical results showed gross underestimation for V_x/V_{mean} < 0.5 and V_x/V_{mean} < 1, but overestimated the results for V_x/V_{mean} < 0.75, compared to experimental data.

The present data are compared to earlier studies in similar-size rectangular channel in Figure 10. The asymmetrical ribbed channel configuration provided substantially smaller LVZs, for the same flow rates, than the rough channel configuration (Figure 10, black symbols). Further comparison with smooth flume data showed comparable LVZ sizes in smooth rectangular flume and ribbed channel. A key difference, however, was the well-marked highly turbulent LVZ beneath the sidewall rib, for all flow conditions, sketched in Figure 2.

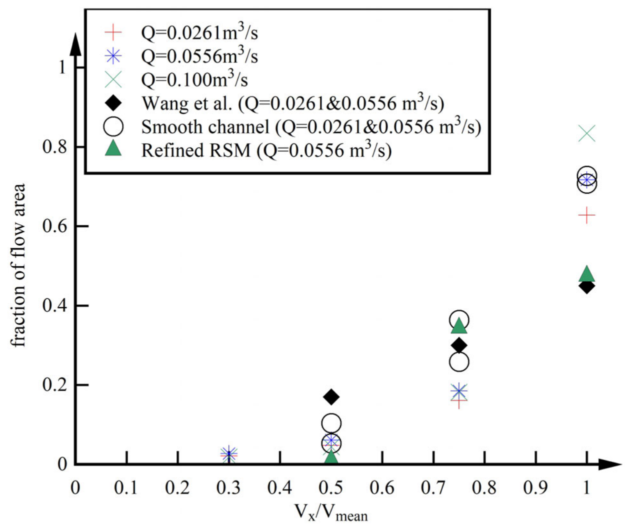

FIGURE 10 Fractions of low velocity regions where V_x/V_{mean} is less than a set value, for different discharges and longitudinal locations—comparison with smooth channel data (Cabonce et al., 2019) (black hollow symbols), asymmetrical rough channel data (Wang et al., 2018) (black symbols) and present CFD using a Reynolds stress model on a refined mesh [Colour figure can be viewed at wileyonlinelibrary.com]

5.2 | Application to upstream fish passage in hydraulic structures

The longitudinal sidewall rib configuration provided a fascinating turbulent flow field, with well-defined LVZs. Such a configuration might be applied to hydraulic structure designs, for example, for the growth of biofilms, enhancement of contaminant mixing in streams or the upstream passage of small-bodied fish in culverts and fish passes. Practically, a number of technical challenges could be linked to the design, manufacturing and installation of the rib, while others would be related to operational considerations.

The secondary motion in the ribbed channel led to a complicated fluid dynamics. The strongest secondary currents were generated in the corner regions, that is, external and internal corners associated with the regions of sharpest curvature, while their effects were seen in most parts of the channel. The secondary currents of Prandtl's second kind have a marked impact on the flow resistance of the channel, as previously reported (Kennedy & Fulton, 1961). Herein, the secondary flow turbulent dissipation induced a 30% reduction in discharge capacity for a given afflux, in average for the experimental flow conditions.

The preferred manufacturing of a ribbed channel would be in factory to ensure that the rib position and alignment are within specifications. In the present study, the rib was installed with an error on the longitudinal rib height less than 1 mm over the entire 12 m. In situ installation of the rib would not meet the same standards, leading possibly to a substantially different hydrodynamic flow field, with adverse impact on the channel operation and function. More, any in situ installation, for example, for retrofitting, would only be feasible in relatively wide channels: B > 1.5 m with internal height greater than 1.5 m.

The current study was conducted with a sharp-edge rib, because sharp edges and corners constitute well-known hydrodynamic discontinuity, conducive of strong secondary currents (Chanson, 2014; Gessner, 1973; Vallentine, 1969). Any rounding of the edges or corner would modify significantly the secondary current motion, impacting the whole turbulent flow field, with adverse impact on the LVZ size and efficiency.

The present tests were undertaken with a 0.05 × 0.05 m^2 square rib, positioned immediately above a 0.05-m high cavity. During

TABLE 1 Experimental measurements of proportion of low-velocity zones in smooth (symmetrical) and asymmetrical rectangular channels

								% Flow area with V_x <			
Ref.	S_o	B (m)	Q (m^3/s)	x (m)	d (m)	V_{mean} (m/s)	$(V_{max})_M$ (m/s)	V_{mean} (%)	0.75 × V_{mean} (%)	0.5 × V_{mean} (%)	0.3 × V_{mean} (%)
Present study Streamwise rib along right sidewall	0	0.50	0.0261	8.0	0.0925	0.592	0.777	62.8	16.1	4.8	2.1
			0.0556	1.9	0.166	0.691	0.77	69.9	15.5	4.8	2.1
				8.0	0.147	0.783	0.903	71.7	18.5	6.1	2.7
				11.9	0.128	0.904	1.045	83.7	25.7	7.2	3.0
			0.100	8.0	0.205	1.000	1.113	83.4	18.2	4.4	1.9
Present CFD study Refined Reynolds stress model	0	0.5	0.0556	8	0.145	0.767	0.908	47.5	34.4	1.2	0.0
Wang et al. (2018) Rough invert and rough left sidewall	0	0.4785	0.0261	8.0	0.129	0.423	0.755	45	30	17	8.5
			0.0556	8.0	0.1743	0.667	0.957				
Cabonce et al. (2017, 2019) Smooth channel	0	0.50	0.0261	8.0	0.096	0.544	0.544	70.8	36.4	5.3	4.6
			0.0556	8.0	0.162	0.686	0.686	72.7	25.9	10.4	7.2

Abbreviations: B, internal channel width; d, water depth; Q, water discharge; S_o, bed slope; V_{mean}, cross-sectional averaged velocity; $(V_{max})_M$, cross-sectional maximum velocity; V_x, longitudinal velocity; x, longitudinal location.

operation, such a cavity would only be suitable to small-bodied fish, less than 0.05 m high. A practical consideration is the risk of siltation and sedimentation. The accumulation of solid particles beneath the rib could lead to a partial or complete blockage of the low velocity regions, because the cavity flow is slow and below current guidelines for self-cleaning (QUDM, 2013). Large debris, including rocks, branches, trees, could also become jammed beneath the rib, obstructing the square cavity and reducing further the channel discharge capacity.

Finally, large boundary shear stresses were observed on the side of the rib, as well as large velocity fluctuations near the edges of the rib. During operation, the rib corners might be subjected to abrasion, leading to some rounding over time. The effects of abrasion, that is, the resulting corner rounding, would change the concentration of shear stresses and velocity fluctuations around the sidewall rib, and in turn the flow field in the cavity beneath the rib.

In summary, the application of sidewall rib to hydraulic structures must be considered with uttermost care. A number of practical engineering considerations showed major technical challenges and issues during design, manufacturing, installation and operation. In many instances, alternative designs should be preferred and implemented, especially at hydraulic structures. For upstream passage of small-bodied fish, these could include asymmetrically roughened culvert barrel (Wang et al., 2018; Wang, Chanson, Kern, & Franklin, 2016; Zhang & Chanson, 2018a) and barrel equipped with small closely spaced triangular corner baffles (Cabonce et al., 2019; Cabonce, Wang, & Chanson, 2018), although the optimum type of boundary treatment might be closely linked to the targeted fish species.

6 | CONCLUSIONS

A detailed hydrodynamic study was conducted in an asymmetrical rectangular channel equipped with a sidewall streamwise rib. Both flow visualisations and flow resistance data showed three-dimensional flow patterns and energy dissipation associated with the rib presence. Strong secondary circulation was observed in the “open” cavity beneath the rib, sketched in Figure 2. The flow resistance was larger than basic skin friction, suggesting in average a 30% reduction in the channel discharge capacity for a given afflux. Numerical CFD modelling showed satisfactory capacity in simulating flows around a longitudinal rib, using a standard $k-\varepsilon$ or RSM, with the latter being more accurate in simulating the hydrodynamics underneath the rib. All CFD models tended to overestimate the flow velocity in the middle of the channel and were overall associated with smaller LVZs as a result.

The results of the current hydrodynamic study suggest that the flow in an asymmetrical channel with a longitudinal rib is complex and delivers relatively small LVZs. The design presents a number of manufacturing, installation and operational issues, including very-high risks of sedimentation and blockage by debris. In many engineering projects, alternative designs should be preferred to assist fish passage at hydraulic structures, including culverts and fish passes, for example, asymmetrically roughened channel and channel equipped with small triangular corner baffles.

ACKNOWLEDGEMENTS

The authors thank Dr John Macintosh (Water Solutions, Australia), Professor Oscar Castro-Orgaz (University of Cordoba, Spain), and Professor Benoit Cushman-Roisin (Dartmouth College, Hanover, NH) for their valuable comments. Hubert Chanson has competing interest and conflict of interest with Craig E. Franklin.

CONFLICT OF INTEREST

Hubert Chanson has competing interest and conflict of interest with Craig E. Franklin.

DATA AVAILABILITY STATEMENT

Some or all data, models, or code that support the findings of this study are available from the corresponding author upon reasonable request. These include the tabular data corresponding to the data presented in Table 1, Figures 5, 8 and 10.

ORCID

Xinqian Leng https://orcid.org/0000-0001-8472-7925
Hubert Chanson https://orcid.org/0000-0002-2016-9650

REFERENCES

Bushnell, D. M., & Mcginley, C. B. (1989). Turbulence control in wall flows. *Annual Review of Fluid Mechanics*, *21*, 1–20.

Cabonce, J., Fernando, R., Wang, H., & Chanson, H. (2017). *Using triangular baffles to facilitate upstream fish passage in box culverts: Physical modelling*." Hydraulic Model Report No. CH107/17. Brisbane, Australia: School of Civil Engineering, The University of Queensland 130 pages (ISBN 978-1-74272-186-6).

Cabonce, J., Fernando, R., Wang, H., & Chanson, H. (2019). Using small triangular baffles to facilitate upstream fish passage in standard box culverts. *Environmental Fluid Mechanics*, *19*(1), 157–179. https://doi.org/10.1007/s10652-018-9604-x

Cabonce, J., Wang, H., & Chanson, H. (2018). Ventilated corner baffles to assist upstream passage of small-bodied fish in box culverts. *Journal of Irrigation and Drainage Engineering*, *144*(8), 0418020, 8 pages. https://doi.org/10.1061/(ASCE)IR.1943-4774.0001329

Carling, P. A., Williams, J. J., Croudace, I. W., & Amos, C. L. (2009). Formation of mud ridge and runnels in the intertidal zone of the Severn Estuary, UK. *Continental Shelf Research*, *29*, 1913–1926.

Chanson, H. (2014). *Applied hydrodynamics: An introduction*. Leiden, The Netherlands: CRC Press, Taylor & Francis Group 448 pages & 21 video movies (ISBN 978-1-138-00093-3).

Choi, H., Moin, P., & Kim, J. (1993). Direct numerical simulation of turbulent flow over riblets. *Journal of Fluid Mechanics*, *255*, 503–539.

Gessner, F. B. (1973). The origin of secondary flow in turbulent flow along a corner. *Journal of Fluid Mechanics*, *58*, Part 1, 1–25.

Goring, D.G., and Nikora, V.I. (2002). "Despiking acoustic Doppler velocimeter data." *Journal of Hydraulic Engineering*, ASCE, Vol. *128*, No. 1, pp. 117–126. Discussion: Vol. 129, No. 6, pp. 484–489.

Itoh, M., Tamano, S., Iguchi, H., Yokota, K., Akino, N., Hino, R., & Kubo, S. (2006). Turbulent drag reduction by the seal fur surface. *Physics of Fluids*, *18*, Paper 065102, 9.

Kennedy, R. J., & Fulton, J. F. (1961). The effect of secondary currents upon the capacity of a straight Open Channel. *Transactions of the Engineering Institute of Canada*, *5*(1), 12–18.

Leng, X., & Chanson, H. (2018). Modelling low velocity zones in box culverts to assist fish passage. In T. C. W. Lau & R. M. Kelso (Eds.), *Proceedings of 21st Australasian fluid mechanics conference, 21AFMC, 10–13 December*. Adelaide, Australia: Paper 547, 4 pages.

Leng, X., & Chanson, H. (2020). Hybrid modelling of low velocity zones in box culverts to assist upstream fish passage. *Environmental Fluid Mechanics*, *20*, 18 pages. https://doi.org/10.1007/s10652-019-09700-1

Macintosh, J.C., and Isaacs, L.T. (1992). "RPT—The roving Preston tube." *Proceedings of the 11th Australasian Fluid Mechanics Conference, 11AFMC*, Hobart, Australia, Vol. II, Paper 8E-1, pp. 1049–1052.

Nezu, I., & Nakagawa, H. (1984). Cellular secondary currents in straight conduits. *Journal of Hydraulic Engineering*, *110*(2), 173–193.

Nitschke, P. (1983). *Experimentelle Undersuchung der turbulenten Stroemung in glatten und laengsgerillten Rohren (Experimental investigation of the turbulent flow in smooth and longitudinal grooved tubes)*. Goettingen, West Germany: Max-Planck Institue fur Stromungsforschung (in German).

Pope, S. B. (2000). *Turbulent flows* (p. 771). Cambridge: Cambridge University Press. https://doi.org/10.1017/CBO9780511840531

QUDM (2013). Queensland urban drainage manual. In *Queensland department of energy and water supply* (3rd ed., p. 459). Brisbane, Australia: Department of Energy and Water Supply, Queensland.

Rodi, W. (1995). Impact of Reynolds-average modelling in hydraulics. *Proceedings Mathematical and Physical Sciences*, *451*(1941), 141–164.

Rodi, W., Constantinescu, G., & Stoesser, T. (2013). *Large-Eddy simulation in hydraulics* (p. 252). Leiden, The Netherlands: IAHR Monograph, CRC Press, Taylor & Francis Group.

Sanchez, P. X., Leng, X., & Chanson, H. (2018). *Fluid dynamics and secondary currents in an asymmetrical rectangular canal with sidewall streamwise rib*." Hydraulic Model Report No. CH113/18. ISBN 978-1-74272-223-8 (p. 158). Brisbane, Australia: School of Civil Engineering, The University of Queensland.

Shvidchenko, A. B., & Pender, G. (2001). Macroturbulent structure of open-channel flow over gravel beds. *Water Resources Research*, *37*(3), 709–719. https://doi.org/10.1029/2000WR900280

Tanaka, K. L. (1999). Debris-flow origin for the Simud/Tiu deposit on Mars. *Journal of Geophysical Research-Planets*, *104*(E4), 8637–8652. https://doi.org/10.1029/98JE02552

Vallentine, H. R. (1969). *Applied hydrodynamics*. London, UK: Butterworths SI edition.

Wang, H., Chanson, H., Kern, P., & Franklin, C. (2016). Culvert hydrodynamics to enhance upstream fish passage: Fish response to turbulence. In G. Ivey, T. Zhou, N. Jones, & S. Draper (Eds.), *Proceedings of 20th Australasian fluid mechanics conference* (p. 4). Perth WA, Australia, 5–8 December, Paper 682: Australasian Fluid Mechanics Society.

Wang, H., Uys, W., & Chanson, H. (2018). Alternative mitigation measures for fish passage in standard box culverts: Physical modelling. *Journal of Hydro-environment Research*, *19*, 214–223. https://doi.org/10.1016/j.jher.2017.03.001

Watson, J., Goodrich, H., Cramp, R., Gordos, M., & Franklin, C. (2018). Utilising the boundary layer to help restore the connectivity of fish habitat and population. *Ecological Engineering*, *122*, 286–294.

Zhang, G., & Chanson, H. (2018a). Effects of step and cavity shapes on aeration and energy dissipation performances of stepped chutes. *Journal of Hydraulic Engineering*, *144*, No. 9, Paper 04018060, 12. https://doi.org/10.1061/(ASCE)HY.1943-7900.0001505

Zhang, G., & Chanson, H. (2018b). Three-dimensional numerical simulations of smooth, asymmetrically roughened, and baffled culverts for upstream passage of small-bodied fish. *River Research and Applications*, *34*(8), 957–964. https://doi.org/10.1002/rra.3346

How to cite this article: Sanchez PX, Leng X, Von Brandis-Martini J, Chanson H. Hybrid modelling of low velocity zones in an asymmetrical channel with sidewall longitudinal rib to assist fish passage. *River Res Applic*. 2020;36:807–818. https://doi.org/10.1002/rra.3600